ACS OMEGA

Open Access

http://pubs.acs.org/journal/acsodf

Article

Flavan-Benzofurans from *Artocarpus lacucha*: Their Intracellular Antioxidant Activity and Molecular Docking to Glutathione Reductase

Weerasak Songoen,* Dominik Wenisch, Michael A. Jakupec, Witthawat Phanchai, Siriphan Sukkhaeng, Lothar Brecker, Johann Schinnerl, Sorachat Tharamak, and Wanchai Pluempanupat

Cite This: *ACS Omega* 2024, 9, 33888−33899

Read Online

ACCESS | Metrics & More | Article Recommendations | Supporting Information

ABSTRACT: Phytochemical investigation of *Artocarpus lacucha* Buch.-Ham (Moraceae) leaves led to the identification of three of the rarely found flavan-benzofuranes named artocarpinol C (**1**), 3-*epi*-artocarpinol C (**2**), and artocarpinol D (**6**) along with six known flavan derivatives. Thus, a total of six artocarpinols are now described. All their chemical structures and absolute configurations were established by one dimensional (1D)- and two-dimensional (2D) NMR, infrared (IR), electronic circular dichroism (ECD), high-resolution electrospray ionisation mass spectrometry (HR-ESI-MS), and optical rotation (OR). Density functional theory (DFT) calculations based on the B3LYP theory level were conducted to determine the stereochemistry at positions 2 and 3 in the C-ring. All compounds exhibited *in vitro* radical scavenging activities, and compounds **3** and **5** demonstrated pronounced intracellular antioxidative effects in colon carcinoma cells (SW480), as determined by the DCFH-DA assay. Compounds **3** and **5** exhibited further high affinities for binding to the active site of human glutathione reductase. These molecular properties are discussed with regard to possible applications.

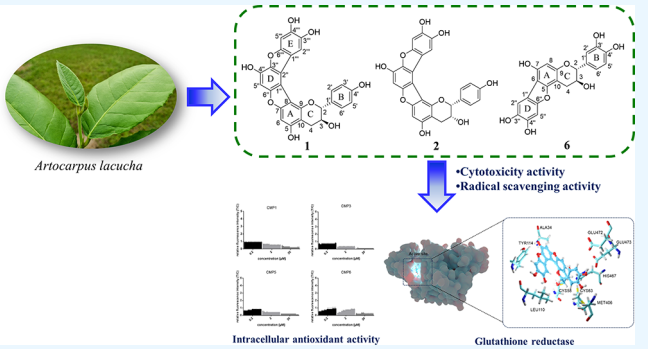

1. INTRODUCTION

The tree species *Artocarpus lacucha* Buch.-Ham (syn *A. lakoocha* Wall. ex Roxb.)(Moraceae) is in Thailand also known as "Ma-Haad". This species is distributed in tropical and subtropical regions of Sount East Asia, where it is applied in traditional folk medicine.[1,2] For example, fruit extracts of *A. lacucha* are used in the treatment of tapeworm infections.[3] Leaf extracts of this plant species are used numerously for wound healing, fever, diarrhea, or even diabetes.[4] Previous studies revealed that this plant species is rich in phenolic compounds such as deoxybenzoins,[5] flavan derivatives,[5] stilbenoids,[6] arylbenzofurans,[7] and flavonoids.[8] Recently, we reported flavan-benzofurans from the leaves and stembark of this species.[9] These compounds consisted of a flavan-3-ol core structure with benzofuran moieties attached and were not yet reported from other *Artocarpus* species. Regarding biological activities, antioxidant,[9] tyrosinase-inhibitory,[10] anticancer,[6,11] antiviral, anti-HIV,[12] and DNA protective[13] activities were reported in previous studies.

Glutathione reductase (GR) is crucial for the reduction of the oxidized form of glutathione disulfide (GSSG) with NADPH to generate the reduced glutathione form (GSH). The ratio of the reduced glutathione form (GSH) to the oxidized form of GSSG is an indicator of cellular health. In red blood cells, the intracellular GSH/GSSG ratio is maintained at a high level by this mechanism. Elevated GSH/GSSG ratio levels lead to intracellular signal transmission, removal of free radicals and reactive oxygen species, and preservation of the intracellular redox state.[14,15] An increased glutathione level can reduce therapeutic effectiveness by inactivating the radical molecules. However, in several diseases, increased levels of GR were found in patients with various tumors, such as lung cancer. Therefore, inhibiting the GR enzyme emerges as an effective therapeutic target to treat diseases related to the oxidative mechanism, such as cancer and malaria, by decreasing the levels of GSH.[16]

In continuation of our previous work,[9] we performed phytochemical investigations of this plant species focusing on flavan-benzofurans, aiming to narrow down potential precursors and getting a deeper insight into the structural diversity of this class of compounds. From the novel compounds, we assessed *in vitro* radical scavenging characteristics, the intra-

Received: April 22, 2024
Revised: June 21, 2024
Accepted: July 2, 2024
Published: July 23, 2024

Table 1. ^{1}H (400 MHz) and ^{13}C NMR (100 MHz) Data of Artocarpinol C (1) 3-*epi*-Artocarpinol C (2) and Artocarpinol D (6) Recorded in CD_3OD; (δ in ppm, J in Hz)

	artocarpinol C (1)		3-*epi*-artocarpinol C (2)		artocarpinol D (6)	
no.	δ_C, type	δ_H (J in Hz)	δ_C, type	δ_H (J in Hz)	δ_C, type	δ_H (J in Hz)
			Flavan-3-ol Moiety			
2	80.5, CH	5.73 d (3.6)	79.6, CH	5.67 d (3.2)	83.3, CH	4.71 d (7.3)
3	67.3, CH	4.54 m	67.2, CH	4.49 m	68.2, CH	4.12 td (7.3, 5.3)
4	25.6, CH_2	2.89 ddd (16.9, 3.9, 1.6)	28.0, CH_2	3.11 dd (16.1, 5.0)	27.9, CH_2	3.13 dd (15.9, 5.3)
		2.67 dd (16.9, 4.5)		2.70 dd (16.1, 7.8)		2.84 dd (15.9, 7.9)
5	156.0, C		155.8, C		157.3, C	
6	91.3, CH	6.63 s	91.4, CH	6.65 s	108.1, C	
7	158.0, C		158.1, C		152.3, C	
8	107.4, C		107.4, C		97.9, CH	6.24 s
9	148.7, C		149.4, C		154.5, C	
10	103.0, C		103.6, C		97.4, C	
1′	131.3, C		130.0, C		132.0, C	
2′	128.0, CH	7.20 d (8.6)	129.9, CH	7.34 d (8.5)	115.2, CH	6.87 d (1.8)
3′	116.3, CH	6.68 d (8.6)	115.7, CH	6.68 d (8.5)	146.2, C	
4′	157.9, C		158.1, C		146.3, C	
5′	116.3, CH	6.68 d (8.6)	115.7, CH	6.68 d (8.5)	116.1, CH	6.77 d (8.1)
6′	128.0, CH	7.20 d (8.6)	129.9, CH	7.34 d (8.5)	120.0, CH	6.75 dd (8.1, 1.8)
			D-Ring			
1″	108.7, C		108.5, C		117.0, C	
2″	119.6, C		119.6, C		108.1, CH	7.26 s
3″	141.8, C		141.8, C		142.8, C	
4″	143.7, C		143.6, C		144.9, C	
5″	98.2, CH	7.00 s	98.1, CH	6.98 s	98.9, CH	6.94 s
6″	153.9, C		153.8, C		151.2, C	
			E-Ring			
1‴	117.6, C		117.4, C			
2‴	111.6, CH	8.44 s	111.8, CH	8.30 s		
3‴	142.5, C		142.4, C			
4‴	147.1, C		147.2, C			
5‴	96.3, CH	7.01 s	96.3, CH	6.98 s		
6‴	152.8, C		152.7, C			

cellular antioxidative effects using the DCFH-DA assay, as well as the cytotoxic activities against the six human cancer cell lines colon cancer (HT-29), oral cavity carcinoma (KB), breast cancer (MCF-7), cervical cancer (HeLa), hepatocellular carcinoma (HepG-2), and leukemia (P388). Additionally, we performed molecular docking studies of the novel compounds to investigate binding interactions to the human glutathione reductase.

2. RESULTS AND DISCUSSION

2.1. Structure Elucidation. Compound **2** was obtained as a brown amorphous solid, and its molecular formula of $C_{27}H_{18}O_9$ at m/z 509.0848 $[M + Na]^+$ was determined by high-resolution-time of flight-electrospray ionization-mass spectrometry (HR-TOF-ESI-MS) (calcd for $C_{27}H_{18}O_9Na$, 509.0849). The ^{1}H and ^{13}C NMR spectra of **2** indicated one sp^3 methylene group, two sp^3 methine groups, eight sp^2 methine groups, and 16 quaternary carbons (Table 1). Further NMR measurements showed signals of a flavan-3-ol core structure with two additional aromatic rings as shown in Figure 1. The one dimensional (1D) and two-dimensional (2D) NMR data of **2** displayed a number of similarities to those of 3-*epi*-artocarpinol A (**4**).[9]

The ^{1}H NMR signals of the A-ring at δ_H 6.65 ppm (H-6), B-ring at δ_H 6.68 ppm (H-2′, 6′) and 7.34 ppm (H-3′, 5′), and C-ring at δ_H 5.67 ppm (H-2), 4.49 ppm (H-3), 3.11 ppm (H-4a), and 2.70 ppm (H-4b) indicated the presence of the flavan-3-ol core structure. A set of AA′BB′-system protons of H-2′, 6′ (δ_H 6.68 ppm, 2H, d, 8.5 Hz) and H-3′, 5′ (δ_H 7.34 ppm, 2H, d, 8.5 Hz) suggested the 1,4-disubstituted phenyl group of the B-ring.

The $^{2,3}J_{H-C}$ coupling in HMBC between H-6 and C-7 (δ_C 158.1 ppm) and C-8 (δ_C 107.4 ppm), as well as H-5″ and C-6″ (δ_C 153.8 ppm) and C-1″ (δ_C 108.5 ppm) assigned the C−C bond connection (C-8 and C-1″) and the ether bond connection (C-7 and C-6″) between A-ring and D-ring. The additional two singlet protons at δ_H 8.30 ppm (H-2‴) and δ_H 6.98 ppm (H-5‴) together with the quaternary carbon signals at δ_C 152.7 ppm (C-6‴), 147.2 ppm (C-4‴), 142.4 ppm (C-3‴), and 117.4 ppm (C-1‴) suggested the presence of trioxygenated benzene of E-ring. The C−C bond connection between C-2″ (D-ring) and C-1‴ (E-ring) was confirmed by the HMBC cross-peaks from H-2‴ (δ_H 8.30 ppm) to C-2″ (δ_C 119.6 ppm). The ether bond linkage between C-3″ and C-6‴ was assigned by the HMBC correlations of H-2‴ (δ_H 8.30 ppm) to C-6‴ (δ_C 152.7 ppm) and H-5″ (δ_H 6.98 ppm) to C-3″ (δ_C 141.8 ppm). The key COSY and HMBC correlations of **2** are shown in Figure 2.

The relative configuration of **2** was deduced through analysis of the NOESY and compared to 3-*epi*-artocarpinol A (**4**). The detection of a NOESY correlation between H-2 and H-2‴ indicated a close proximity location of these two protons (2.38

https://doi.org/10.1021/acsomega.4c03865
ACS Omega 2024, 9, 33888−33899

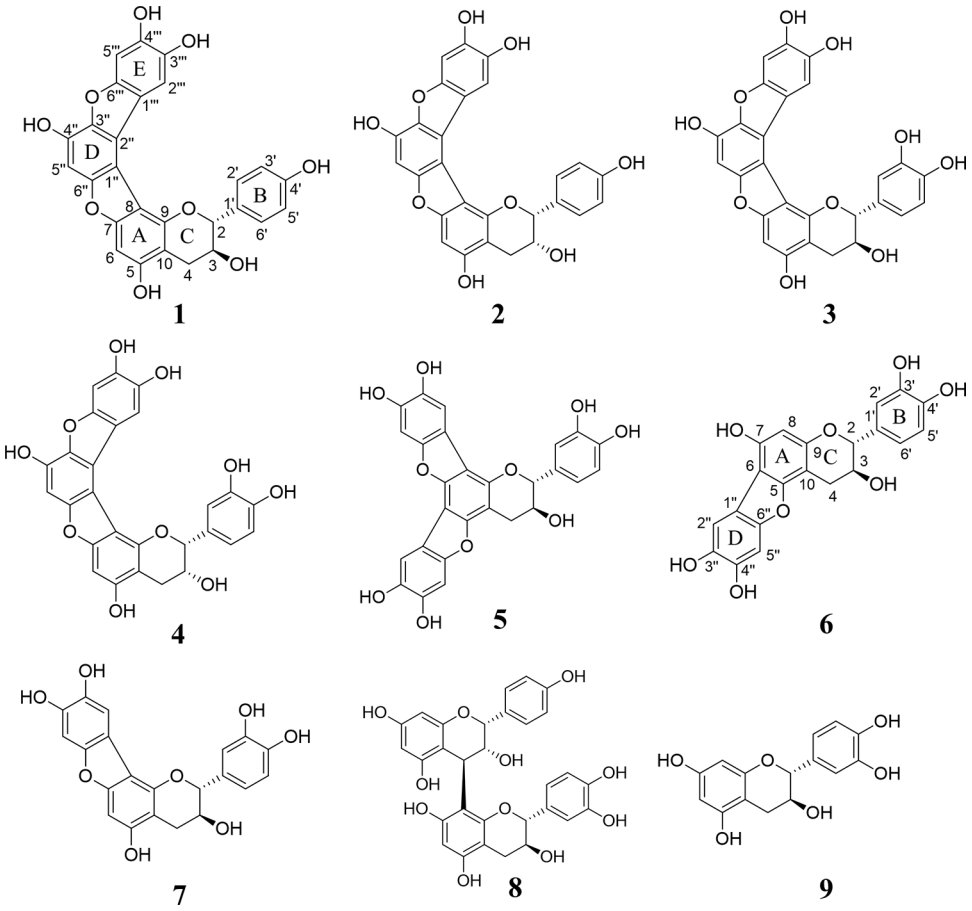

Figure 1. Chemical structures of artocarpinol C (**1**), 3-*epi*-artocarpinol C (**2**), artocarpinol A (**3**), 3-*epi*-artocarpinol A (**4**), artocarpinol B (**5**), artocarpinol D (**6**), gambircatechol (**7**), gambiriin C (**8**), and (+)-catechin (**9**) isolated from the leaves of *A. lacucha*.

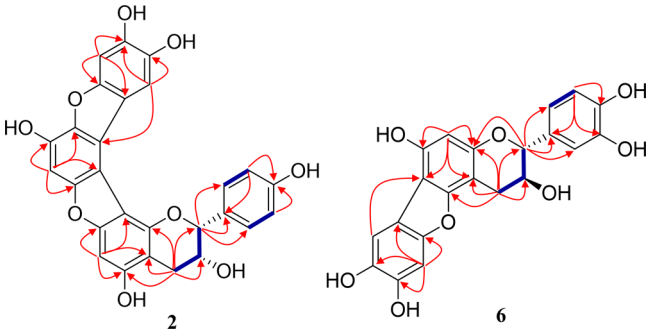

Figure 2. Key COSY (bold blue lines) and HMBC correlations (red arrows) of 3-*epi*-artocarpinol C (**2**) and artocarpinol D (**6**).

Å from density functional theory (DFT) calculation) as shown in Figure 3. Moreover, a small coupling constant value of H-2 (δ_H 5.67 ppm, 1H, d, 3.2 Hz) as well as the NOESY correlation between H-2 and H-3 and H-4a indicated a spatial closeness of these protons, which are located in the same side (2,3-*cis* structure). The absolute configuration of **2** was assigned by comparing the observed optical rotation value with the theoretical calculation by the density functional theory (DFT) with six d-type Cartesian−Gaussian polarization functions (6-31G(d,p)) in Gaussian 09.[17,18] The observed optical rotation of **2** (−337.5) was significantly close to the theoretical calculation (−343.3). In addition, the absolute configuration of **2** was also supported through electronic circular dichroism (ECD) measurement, which exhibited a similar pattern to the calculated ECD spectra by DFT calculation, in particular with a maximum in the region of 260 nm (Figure 4b). Any deviations in other frequency ranges may be due to spatial repulsion effects between positions 1 and 2‴, which may give the molecule a helical character. However, this has not been investigated further. Hence, the absolute configuration of compound **2** was determined as 2*R* and 3*R* configurations. Based on the spectroscopic and spectrometric data, compound **2** was identified and named as 3-*epi*-artocarpinol C.

Compound **1** was obtained as a brown amorphous solid with a molecular formula of $C_{27}H_{18}O_9$. The molecular ion at *m*/*z* 509.0874 $[M + Na]^+$ was determined by HR-TOF-ESI-MS (calcd for $C_{27}H_{18}O_9Na$, 509.0849). The overall ^1H and ^{13}C NMR spectra of compound **1** strongly corresponded to those of compound **2**. The indication of one sp^3 methylene group (H-4a, δ_H 2.89 ppm and H-4b, δ_H 2.67 ppm), two sp^3 methine groups (H-2, δ_H 5.73 ppm and H-3, δ_H 4.54 ppm), eight sp^2 methine groups, and 16 quaternary carbons assigned the presence of a flavan-3-ol core structure with two additional aromatic rings (Figure 1). The presence of D-ring and E-ring was confirmed by their corresponding ^1H NMR signals of H-5″ (δ_H 7.00 ppm, 1H, s) as well as H-2‴ (δ_H 8.44 ppm, 1H, s) and H-5‴ (δ_H 7.01 ppm, 1H, s), respectively.

Comparable to compound **2**, the high-field shifted peak of H-2′ from δ_H 7.34 ppm to δ_H 7.20 ppm and H-4a from δ_H 3.11 ppm to δ_H 2.89 ppm indicated the shielded proton signal of both positions which located farther from the −OH group at

https://doi.org/10.1021/acsomega.4c03865
ACS Omega 2024, 9, 33888−33899

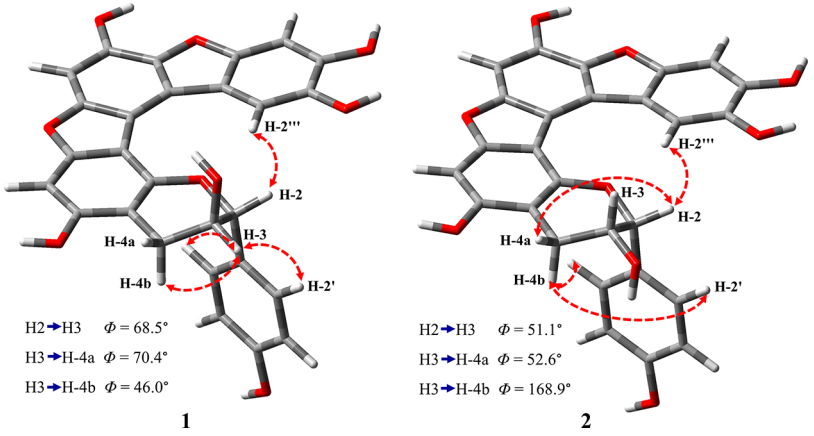

Figure 3. Three-dimensional structure and key NOESY correlations of artocarpinol C (**1**) and 3-*epi*-artocarpinol C (**2**).

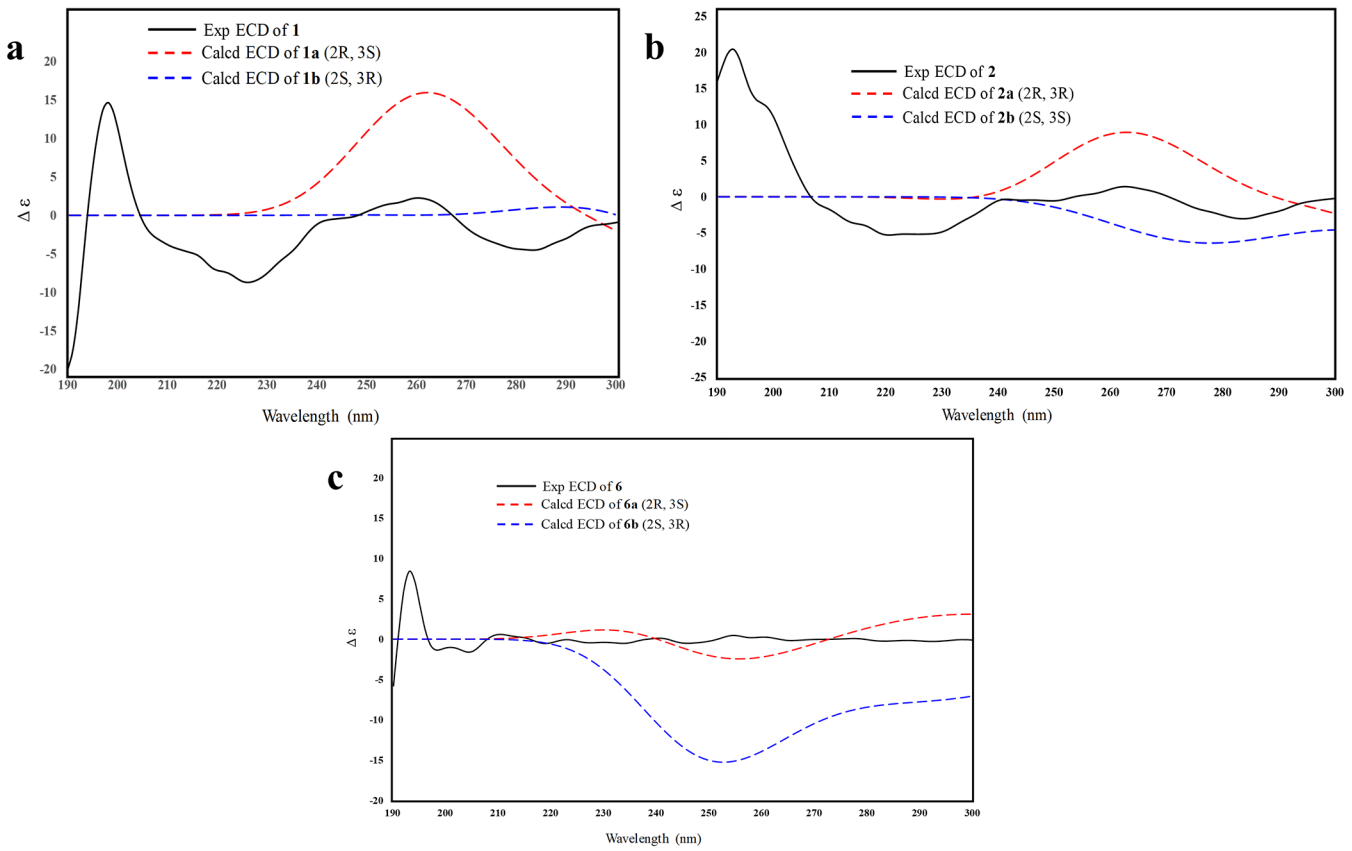

Figure 4. Experimental ECD and calculated spectra of artocarpinol C (**1**), 3-*epi*-artocarpinol C (**2**), and artocarpinol D (**6**). (a) Experimental ECD spectrum of **1** and calculated ECD spectrum of **1**-enantiomer (2*S*, 3*R*). (b) Experimental ECD spectrum of **2** and calculated ECD spectrum of **2**-enantiomer (2*S*, 3*S*). (c) Experimental ECD spectrum of **6** and calculated ECD spectrum of **6**-enantiomer (2*S*, 3*R*).

position 3 (2,3-*trans* structure). On the other hand, the closer −OH group (position 3) and H-2 was assigned by the low-field shifted peak of H-2 from δ_H 5.67 ppm to δ_H 5.73 ppm and C-2 from δ_C 79.6 ppm to δ_C 80.5 ppm (deshielded proton and carbon signals). However, the $^3J_{H-H}$ coupling constants between the protons at positions 2 and 3 in both compounds **1** and **2** are complex. As shown in Figure 3, the C-ring is not in a perfect chair conformation. The sp^2 hybridization at positions 9 and 10, along with the steric influences of other parts of the molecule, leads to very similar H−C−C−H torsion angles between positions 2 and 3 in compounds **1** (2,3-*trans* structure; 68.5°) and **2** (2,3-*cis* structure; 51.1°). These configurational and conformational differences cannot, be clearly distinguished by the coupling constants of 3.6 Hz for compound **1** and 3.2 Hz for compound **2**. However, in compound **1** (2,3-*trans* structure), the proton at position H-3 forms H−C−C−H torsion angles of 70.4 and 46.0° with protons H-4a and H-4b, respectively (Figure 3). This leads to two relatively small $^3J_{H-H}$ coupling constants (4.5 and 3.9 Hz). In contrast, in compound **2** with a 2,3-*cis* structure, the corresponding H−C−C−H torsion angles are 52.6 and 168.9°. This results in a small $^3J_{H-H}$ coupling constant of 5.0 Hz (H-4a), and a significantly larger one of 7.8 Hz (H-4b). These variations in coupling constants therefore strongly support the

https://doi.org/10.1021/acsomega.4c03865
ACS Omega 2024, 9, 33888−33899

different stereochemistry of the two compounds **1** and **2** (Figure 3). However, the slight shift of proton and carbon signals at position 2, as well as the slight difference in the coupling constant of H-2 in both compounds **1** and **2**, could be influenced by the close proximity of the aromatic E-ring, as depicted in Figure 3. The effect of the close proximity of the E-ring to the C-ring is further evidenced by the appearance of a rather downfield proton signal of H-2‴ in both compound **1** (δ_H 8.44 ppm) and compound **2** (δ_H 8.30 ppm). These protons are situated close to the oxygen atom (ether bond) in the C-ring. Moreover, the relative configuration of **1** was also assigned by NOESY correlation as shown in Figure 3. The NOESY cross peak between H-2 (δ_H 5.73 ppm) and H-2‴ (δ_H 8.44 ppm) indicated a close proximity of these two protons. In addition, the detection of NOESY correlation between H-3 (δ_H 4.54 ppm) and only H-4b (δ_H 2.67 ppm) indicated that these two protons were located in the same side. The absolute configuration of **1** was confirmed by analysis of the optical rotation value compared to the theoretical calculation; the results −370.8 (calcd = −374.4) were significantly close. Moreover, the ECD measurement revealed that the experimental ECD spectra of **1** exhibited a similar pattern to the calculated ECD spectra obtained from DFT calculation, in particular with a maximum in the region of 260 nm as depicted in Figure 4a. Deviations in other frequency ranges may have the same causes as discussed for **2**. Therefore, the absolute configuration of compound **1** was determined as 2*R* and 3*S* configurations. Based on these data, this yet undescribed flavan-3-ol derivative is named artocarpinol C.

Compound **6** with the molecular formula $C_{21}H_{16}O_8$ was obtained as a brown amorphous solid. The molecular ion at *m*/*z* 419.0737 $[M + Na]^+$ by HR-TOF-ESI-MS corresponded to the calculation for $C_{21}H_{16}O_8Na$ (*m*/*z* 419.0743). The ^1H and ^{13}C NMR spectra and multiplicities of nuclei (Table 1) showed the signals of one sp^3 methylene group, two sp^3 methine groups, six sp^2 methine groups, and twelve quaternary carbons. Further, 1D and 2D NMR measurements assigned the presence of a flavan-3-ol core structure with one additional aromatic ring similar to gambircatechol (**7**). The characteristic ^1H NMR signal of A-ring at δ_H 6.24 ppm (H-8), B-ring at δ_H 6.87 ppm (H-2′), 6.77 ppm (H-5′), and 6.75 ppm (H-6′), and C-ring at δ_H 4.71 ppm (H-2), 4.12 ppm (H-3), 3.13 ppm (H-4a), and 2.84 ppm (H-4b) indicated the presence of a catechin core structure. The additional aromatic ring (D-ring) was assigned by the ^1H NMR signal at δ_H 7.26 ppm (H-2″) and δ_H 6.94 ppm (H-5″). The connection between the A-ring and D-ring was confirmed by HMBC correlation. The disappearance of the singlet proton at position 6, as well as the $^3J_{H-C}$ coupling in HMBC from H-8 (δ_H 6.24 ppm) and H-2″ (δ_H 7.26 ppm) to C-6 (δ_C 108.1 ppm) indicated the C−C bond connection between C-6 (A-ring) and C-1″ (D-ring). In addition, the ether bond between C-5 in the A-ring and C-6″ in the D-ring was assigned by the HMBC correlation of H-2″ and H-5″ to C-6″ together with the HMBC correlation of H-4a to C-5. The key COSY and HMBC correlations of **6** are showed in Figure 2.

The relative configuration of compound **6** was deduced according to the well-known compound (+)-catechin (**9**). In addition, the $^1H-^1H$ coupling constant data and the NOESY correlation were used. The key NOESY correlation between H-2′ (δ_H 6.87 ppm), H-6′ (δ_H 6.75 ppm), and H-3 (δ_H 4.12 ppm) indicated a spatial closeness of these protons. The detection of NOESY correlation between H-2 (δ_H 4.71 ppm) and H-4b (δ_H 2.84 ppm) showed that both protons were located in immediate proximity. The absolute configuration of **6** was also confirmed by comparing the observed optical rotation value and the theoretical calculation. The observed optical rotation value of 105.0 was significantly close (calcd = 101.5). Additionally, the absolute configuration of **6** was investigated via ECD measurement. The measured ECD spectra of compound **6** show no clear maxima in the indicative region (250 to 260 nm). With respect to the argumentation given for the ECD of **2**, it is more likely that the ECD of the 2*R* and 3*S* configurations is present here while superimposed by other effects (Figure 4c). Hence, the absolute configuration of compound **6** was determined as 2*R* and 3*S* configurations in particular with respect to the optical rotation value. According to the plant source, this compound was named artocarpinol D.

In addition, the six known flavan-3-ol derivatives, artocarpinol A (**3**), 3-*epi*-artocarpinol A (**4**), artocarpinol B (**5**), gambircatechol (**7**), gambiriin C (**8**), and (+)-catechin (**9**) were isolated and identified by comparing their spectroscopic and spectrometric data with previous reports.[9,19,20] Compounds **3**, **4**, **5**, **7**, and **9** were recently reported.[9] Compound **8** was isolated from the leaves and twigs of *Uncaria gambir* (W.Hunter) Roxb. (Rubiaceae)[21] and is now found in the leaves of *A. lacucha* as well.

2.2. Radical Scavenging Activity of Isolated Compounds by DPPH and ABTS Assays. Radical scavenging activity of isolated compounds **1**, **2**, **3**, **5**, **6**, **7**, and **8** was determined by DPPH and ABTS assays.[22] For the DPPH assay, compounds **3** (EC_{50} = 10.85 ± 0.84 μM) and **5** (EC_{50} = 12.31 ± 1.04 μM) displayed higher radical scavenging activity compared to the other isolated compounds as well as ascorbic acid (EC_{50} = 24.88 ± 3.11 μM) and trolox (EC_{50} = 37.61 ± 2.06 μM) as shown in Table 2. Comparing compounds **1**, **2**, **3**, and **5**, which consist of the same core structure, reveals that the *ortho*-hydroxyl groups at positions 3′ and 4′ could in particular affect the radical scavenging activity of compounds **3** and **5**. In the ABTS assay, all tested compounds exhibited higher radical scavenging activity than the positive control ascorbic acid (EC_{50} = 7.25 ± 0.47 μM). Among all of the compounds, **3** and **7** showed the most potent radical scavenging properties with EC_{50} values of 0.88 ± 0.09 and 0.89 ± 0.16 μM, respectively.

Table 2. DPPH and ABTS Radical Scavenging Activity of Compounds 1, 2, 3, 5, 6, 7, and 8[a]

compound	DPPH EC_{50} (μM)	ABTS EC_{50} (μM)
1	25.20 ± 2.81	1.27 ± 0.15
2	21.27 ± 2.29	3.56 ± 0.39
3	10.85 ± 0.84	0.88 ± 0.09
5	12.31 ± 1.04	2.55 ± 0.20
6	30.56 ± 1.54	2.21 ± 0.22
7	23.87 ± 2.75	0.89 ± 0.16
8	26.96 ± 3.47	1.44 ± 0.13
ascorbic acid	24.88 ± 3.11	7.25 ± 0.47
trolox	37.61 ± 2.06	13.86 ± 0.93

[a]All results are expressed as mean ± SD; *n* = 3 for all groups.

2.3. Antioxidative Effects of Compounds 1, 3, 5, and 6 in SW480 Cells Using the DCFH-DA Assay. To study the intracellular antioxidative effects, the isolated compounds **1**, **3**, **5**, and **6** were selected to investigate their effects on reactive oxygen species (ROS) levels in the colon carcinoma cell line SW480 using the fluorimetric 2′,7′-dichlorodihydrofluorescein

https://doi.org/10.1021/acsomega.4c03865
ACS Omega 2024, 9, 33888−33899

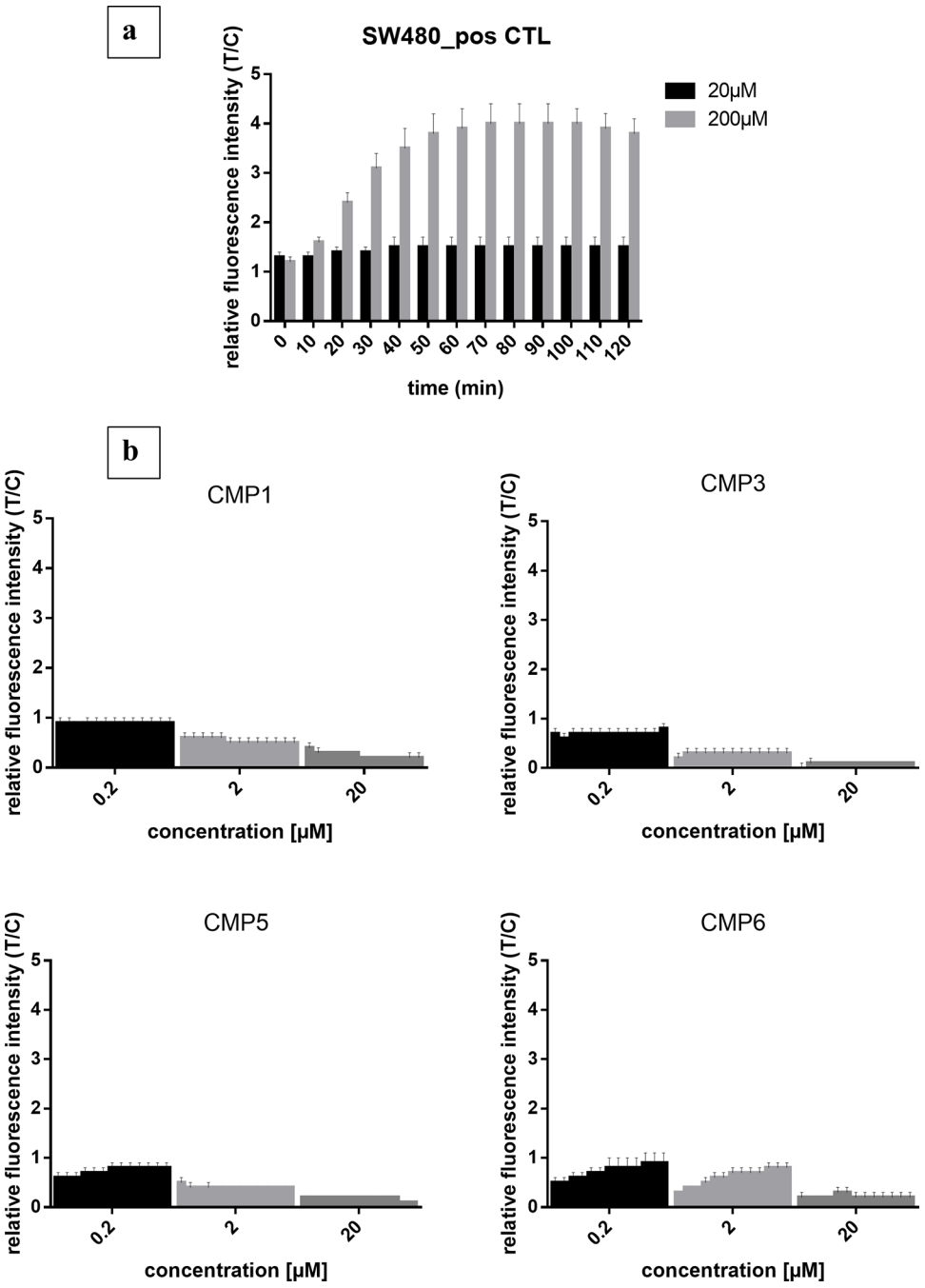

Figure 5. Cellular ROS levels upon treatment with compounds **1**, **3**, **5**, and **6** and/or TBHP (pos. CTL) monitored by the DCFH-DA assay. (a) SW480 cells exposed for 2 h to TBHP at concentrations of 20 and 200 μM. (b) SW480 cells exposed for 2 h to compounds **1**, **3**, **5**, and **6** at concentrations of 0.2, 2, and 20 μM. Values are means ± standard deviations from at least three independent experiments. Values of 0 and 1 correspond to blanks (medium only) and untreated controls, respectively, for each time point.

diacetate (DCFH-DA) assay.[23] Cells were incubated for a period of 2 h with three different concentrations of each compound.[24] As a positive control, *tert*-butyl-hydroperoxide (TBHP) was used. For all test compounds, antioxidative effects dependent on compound concentration could be observed by a decrease in ROS levels (Figure 5). The higher the concentration of the compound, the less ROS were detectable. What appears as a slight increase in those levels at the lowest concentration (0.2 μM) of compounds **5** and **6** actually reflects ROS levels never exceeding a value of 0.9 relative to the negative control.

For the higher concentrations 2 and 20 μM, distinct decreases in ROS levels were observed, most prominent for compounds **3** and **5**, while compound **6** seemed to be the least antioxidative of the tested substances. Comparison of **1** and **3**, only differing by the absence or presence of one more hydroxyl group in the *ortho* position, suggests that the additional hydroxyl group of the latter compound is favorable for antioxidative effect. On the other hand, compounds **5** and **6** differ by the presence or absence of a third catechol moiety, the presence of which results in improved antioxidative properties of compound **5**, which was in line with expectations. To what extent the pseudo-planar chemical structures of **3** and

https://doi.org/10.1021/acsomega.4c03865
ACS Omega 2024, 9, 33888−33899

Table 3. Cytotoxicity (% inhibition of growth) of Compounds 2, 3, 5, 6, and 7 in Six Human Tumor Cell Lines[a,b]

compound	HT29	KB	MCF7	P388	HeLa	HepG2
2	18.14 ± 0.47	9.09 ± 0.03	13.22 ± 0.36	10.60 ± 0.38	1.37 ± 0.44	9.08 ± 0.66
3	0.65 ± 0.37	11.72 ± 0.87	42.23 ± 0.73	89.47 ± 0.29	20.40 ± 0.07	6.89 ± 0.41
5	16.61 ± 0.47	16.23 ± 0.35	37.76 ± 0.38	38.94 ± 0.32	10.95 ± 0.28	NA
6	14.65 ± 0.61	11.85 ± 0.16	33.17 ± 0.06	18.50 ± 0.58	21.74 ± 0.21	5.77 ± 0.44
7	30.72 ± 0.69	16.84 ± 1.38	39.62 ± 0.12	87.26 ± 0.17	18.14 ± 0.15	8.49 ± 0.08

[a]The tested concentration was determined at 100 μg mL^{-1}. All results are means ± SDs; n = 3 for all groups. [b]NA = not active.

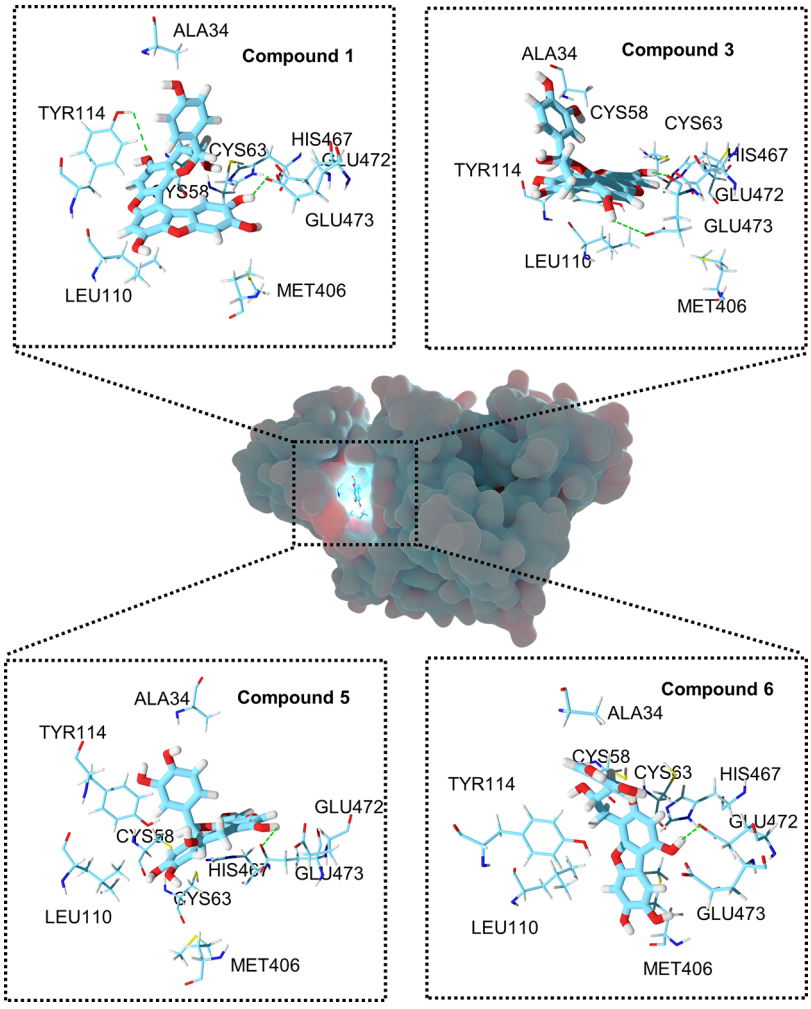

Figure 6. Proposed docking modes of compounds 1, 3, 5, and 6 within the active site of glutathione reductase (PDB 2gh5). Hydrogen bonds are shown with green dashed lines.

5, in particular, contribute to higher uptake by passive diffusion through cell membrane and their elevated impact on radical scavenging activity remains unclear. Nevertheless, these activities also suggest radical scavenging activities *in vivo*. Overall, the obtained results are in good accordance with those obtained by the DPPH and ABTS assays.

2.4. Cytotoxicity Activity. Based on the availability of isolated substances, compounds 2, 3, 5, 6, and 7 were screened on their cytotoxicity in six human cancer cell lines originating from colon cancer (HT-29), oral cavity carcinoma (KB), breast cancer (MCF-7), cervical cancer (HeLa), hepatocellular carcinoma (HepG-2), and leukemia (P388) using the MTT assay with an incubation time of 24 h. Compounds 3 and 7 showed significant cytotoxicity at 100 μg mL^{-1} in the leukemia cancer cell line P388 with inhibition values of 89.47 ± 0.29 and 87.26 ± 0.17%, while the other compounds showed negligible activity (% inhibition values <50%), as shown in Table 3. Further analysis of the half-maximal inhibitory concentration (IC_{50}) in the leukemia cell line showed that both compounds exhibit moderate cytotoxicity with IC_{50} values of 101.23 ± 0.03 and 99.28 ± 0.23 μM, respectively.

2.5. Docking Studies. The enzyme glutathione reductase belongs to the group of flavin-dependent enzymes and catalyzes the reduction of glutathione disulfide to glutathione.[25] The peptide glutathione (γ-L-glutamyl-L-cysteinylglycin) plays a crucial role in defense against reactive oxygen species (ROS) in organisms. In the active site of glutathione reductase (GR), a profound pocket is present, comprising amino acids such as Tyr-114, Cys-58, His-467, etc. The selected compounds 1, 3, 5, and 6, based on their *in vitro*

https://doi.org/10.1021/acsomega.4c03865
ACS Omega 2024, 9, 33888−33899

radical scavenging properties (see Sections 2.2 and 2.3), docked into the GR active site. In this study, we conducted the GR simulations to observe potential interactions of the selected compounds within the active site of GR. Basically, binding interaction among protein−ligand arises from non-covalent bonding, encompassing van der Waals interactions, hydrogen bonds, and electrostatic interactions. The hydroxyl groups present in the molecules are capable to establish hydrogen bonds with amino acids located in the active site of GR. In the case of hydrogen bonds in the active site, the hydroxyl groups of **1** established two hydrogen bonds with Tyr-114 (3.2 Å) and Glu473 (2.8 Å). Compound **3** formed a pair of hydrogen bonds with Glu-472 (2.2 Å) and Glu-473 (2.6 Å). One hydroxyl group of **5** is able to form a hydrogen bond with Glu-473 (2.5 Å). Compound **6** formed one hydrogen bond with Glu-472 (2.0 Å). The docking of selected compounds into the active site of GR and the distances are shown in Figure 6 and Table 4, respectively. See Figure S49 for additional details about the computations of the H-bond numbers and distances between protein residues and compounds.

Table 4. Docking Results of Compounds 1, 3, 5, and 6 with Glutathione Reductase

			energy (kJ mol^{-1})		
compound	residues	distance (Å)	E_{elec}	E_{vdW}	$E_{binding}$
1	His-467	3.5	−78.42	−121.27	−81.18
	Glu-472	4.2			
	Tyr-114[a]	3.2			
	Glu-473[a]	2.8			
	Met-406	6.0			
3	His-467	3.2	−88.58	−188.89	−103.80
	Glu-472[a]	2.2			
	Tyr-114	42			
	Glu-473[a]	2.6			
	Met-406	5.9			
5	His-467	5.4	−86.97	−183.32	−102.20
	Glu-472	4.4			
	Tyr-114	36			
	Glu-473[a]	2.5			
	Met-406	2.5			
6	His-467	2.5	−81.09	−31.24	−89.62
	Glu-472[a]	2.0			
	Tyr-114	36			
	Glu-473	4.1			
	Met-406	2.8			

[a]= Hydrogen bond.

Apart from hydrogen bonding, we observed van der Waals interactions (E_{vdW}) and electrostatic interactions (E_{elec}). Compound **1** indicates that E_{elec} is −78.42 kJ mol^{-1}, and E_{vdW} is −121.27 kJ mol^{-1}. These values collectively contribute to the calculation of the binding energy ($E_{binding}$ = −81.17 kJ mol^{-1}). For compound **3**, the E_{elec} is estimated at −88.58 kJ mol^{-1}, E_{vdW} is estimated at −188.89 kJ mol^{-1}, and $E_{binding}$ is calculated to be −103.8 kJ mol^{-1}. Compound **5** is associated with E_{elec} of −86.97 kJ mol^{-1}, E_{vdW} estimated at −183.32 kJ mol^{-1}, and $E_{binding}$ calculated as −102.2 kJ mol^{-1}. Finally, compound **6** demonstrates E_{elec} of −81.09 kJ mol^{-1}, E_{vdW} of −31.24 kJ mol^{-1}, and $E_{binding}$ of −89.62 kJ mol^{-1} as illustrated in Table 4.

Furthermore, specific parameters, such as the root-mean-square deviation (RMSD), are exacted from the trajectories of each complex. The mean RMSD values of complexes of protein-compound **3**, protein-compound **5**, protein-compound **6**, and protein-compound **1** were 0.16, < 0.28 < 0.54, and < 0.69 Å, respectively, as illustrated in Figure 7. This suggests

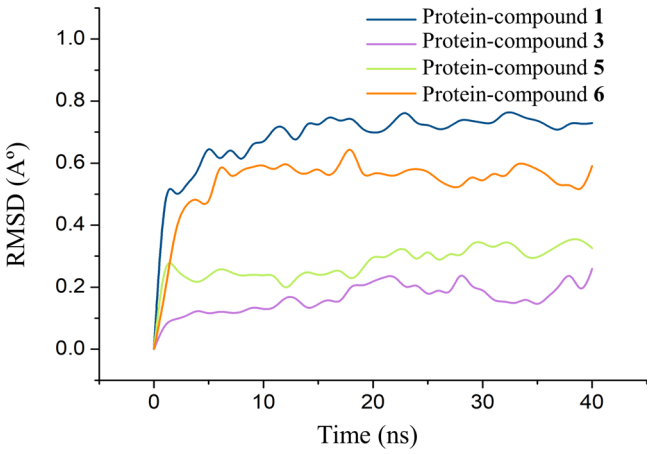

Figure 7. RMSD for four protein-compound complexes during the MD simulations.

that the molecules remained remarkably stable throughout the MD simulations. Based on these findings, Glu-472 and Glu-473 exhibit a robust binding association with compounds, primarily through hydrogen bonding. The lower binding energy observed in compounds **3** and **5** suggests a strong influence of these residues in stabilizing the protein complex within the active site of GR.

3. CONCLUSIONS

Three new flavan-benzofuran derivatives, along with six known compounds, were isolated and identified from the leaves of *A. lacucha*. These new members of flavan-benzofuranes are likely formed by the dimerization of catechin between position 6 or 8 in the A-ring of one catechin molecule and position 6′ in the B-ring of a second catechin molecule. Further, dimerization of two catechins between position 8 and position 4 is also possible in *A. lacucha*. Additionally, the variation of one- and two-hydroxy group substitutions in the B-ring was found. The pseudo-planar chemical structures may also enhance intracellular radical scavenging activities, as observed for **3** and **5**. Both compounds also exhibited high affinities for binding in the active site of human glutathione reductase, as shown by a molecular docking study. The obtained results encourage further investigation of flavan-benzofurans and related compounds in *Artocarpus* as well as in related genera to shed further light on the significance of these compounds for the plants as well as for possible applications. The importance of these compounds for chemotaxonomy within *Artocarpus* remains unclear due to the lack of broader-based studies. These compounds represent a remarkable class of compounds, particularly due to their large quasi-planar molecular structure and the bioactivities described. This could be of interest as health-promoting candidates in the pharmaceutical sector.

4. EXPERIMENTAL SECTION

4.1. General Experimental Procedures. The ultraviolet (UV) spectra were measured by UV−visible spectrophotom-

https://doi.org/10.1021/acsomega.4c03865
ACS Omega 2024, 9, 33888−33899

eters (GENESYS 10S series, Thermo Scientific). The Fourier transform-infrared (FT-IR) spectra were recorded on a Fourier transform infrared spectrometer (Spectrum 400 PerkinElmer). The optical rotation (OR) was recorded using a Polarimeter P3000 (A.KRÜSS Optronic, Germany). ECD spectra were measured by a circular dichroism spectrometer (JASCO, J-815). High-resolution ESI-MS spectra were recorded on a QTOF high-resolution mass spectrometer, micrOTOF-Q III (Bruker Daltonics, Bremen, Germany). 1D and 2D NMR spectra were recorded on a Bruker 400 MHz AVANCE III HD spectrometer at 400 MHz (^{1}H) and 100 MHz (^{13}C). Spectra were processed with MestReNova 14.1.2 software. Chemical shifts (δ) and coupling constants (J) are given in ppm and Hz, and CH_3, CH_2, CH, and C_q are indicated by the multiplicities, respectively. High-performance liquid chromatography (HPLC) analyses were performed on Agilent 1100 series with UV-diode array detection using a Hypersil BDS-C18 column, 250 mm × 4.6 mm, 5 μm particle size, at a flow rate of 1.0 mL min^{-1}. The wavelength of detection was set at 254 nm. Silica gel column chromatography was obtained using Merck silica gel 60 (40−63 μm) and monitored by silica gel 60 F_{254} plates, with a layer thickness of 0.2 mm (Merck). The purification based on size exclusion chromatography (SEC) was done by using Sephadex LH-20 (GE Healthcare) eluted with MeOH. The Gaussian 09 software package (Gaussian 09, Revision B.01, 2016) was used for energy optimization and frequency calculations of a single molecule. The hybrid function Becke−3−Lee−Yang−Parr (B3LYP) and double-ζ polarized basis set with six d-type Cartesian−Gaussian polarization functions (6-31G(d,p)) were used.

4.2. Plant Material. Leaves of *A. lacucha* were collected from Udonthani, Thailand, in January 2022 (17°07′25.8″N, 102°33′41.6″E). A voucher specimen (BK No. 070908) has been deposited at the Plant Varieties Protection Department of Agriculture, Bangkok, Thailand.

4.3. Extraction and Isolation. The air-dried leaves of *A. lacucha* (8.4 kg) were ground and extracted with MeOH (3 × 7 days). The methanolic extracts were filtered, pooled, and evaporated to yield a dry residue (1.2 kg). The crude extract was successively partitioned with *n*-hexane, dichloromethane, ethyl acetate, and distilled water. The ethyl acetate fraction (95.0 g) was chromatographed by a silica gel column chromatography using a solvent mixture of 20% EtOAc in petrol ether to 80% MeOH to afford 18 fractions. Fraction 10 (3.5 g) was further purified by silica gel column chromatography using isocratic elution of dichloromethane/ethyl acetate/methanol (1:6:1) to give six subfractions. Subfraction 2 (1.9 g) was purified over Sephadex LH20 and eluted with MeOH, yielding compounds **1** (2.6 mg), **2** (25.0 mg), **5** (75.0 mg), **6** (5.7 mg), **7** (13.6 mg), and **9** (48.9 mg). The combined fractions 11 and 12 (10.0 g) were separated over a silica gel column to get 7 subfractions. Then, subfraction 5 (1.6 g) was purified by Sephadex column and eluted with MeOH, affording 115.0 mg of **3**, 25.0 mg of **4**, and 52.1 mg of **8**.

4.4. Isolated Compounds. *4.4.1. Artocarpinol C (**1**).* Brown amorphous solid; $[\alpha]_D^{25}$ = −370.8 (c 0.6, CH_3OH); UV λ_{max}(MeOH) nm (log ε): 227 (4.74), 264 (4.48), 287 (4.39), 321 (4.47), 339 (4.38), 354 (4.37); IR (ATR) ν_{max} 3391, 1616, 1515, 1457, 1235, 1162, 1066 cm^{-1}; ^{1}H and ^{13}C NMR data see Table 1; HR-TOF-ESI-MS m/z 509.0874 $[M + Na]^+$ (calcd for $C_{27}H_{18}O_9Na$, 509.0849). The 1D and 2D NMR spectra and mass spectra are given in the Supporting Data File.

*4.4.2. 3-epi-Artocarpinol C (**2**).* Brown amorphous solid; $[\alpha]_D^{25}$ = −337.5 (c 0.8, CH_3OH); UV λ_{max}(MeOH) nm (log ε): 224 (4.37), 265 (4.13), 323 (4.10), 339 (4.05), 354 (4.05); IR (ATR) ν_{max} 3243, 2925, 1609, 1457, 1153, 1048, 799 cm^{-1}; ^{1}H and ^{13}C NMR data see Table 1; HR-TOF-ESI-MS m/z 509.0848 $[M + Na]^+$ (calcd for $C_{27}H_{18}O_9Na$, 509.0849). The 1D and 2D NMR spectra and mass spectra are given in the Supporting Data File.

*4.4.3. Artocarpinol D (**6**).* Brown amorphous solid; $[\alpha]_D^{25}$ = 105.0 (c 1.0, CH_3OH); UV λ_{max}(MeOH) nm (log ε): 226 (4.54), 269 (4.17), 287 (4.11), 324 (4.10); IR (ATR) ν_{max} 3364, 2930, 1614, 1515, 1455, 1283, 1153, 1115, 823 cm^{-1}; ^{1}H and ^{13}C NMR data see Table 1; HR-TOF-ESI-MS m/z 419.0737 $[M + Na]^+$ (calcd for $C_{21}H_{16}O_8Na$, 419.0743). The 1D and 2D NMR spectra and mass spectrum are given in the Supporting Data File.

*4.4.4. Gambiriin C (**8**).* ^{1}H NMR (400 MHz, CD_3OD): δ 7.26 (2H, d, J = 8.6 Hz, H-2″, 6″), 6.88 (1H, d, J = 1.9 Hz, H-6′), 6.85−6.77 (3H, m, H-5″, 6″, 3′), 6.75 (1H, dd, J = 8.2, 2.0 Hz, H-2′), 6.10 (1H, d, J = 2.3 Hz, H-6), 6.04 (2H, d, J = 2.2 Hz, H-8), 5.02 (1H, s, H-2a), 4.66−4.59 (2H, m, H-4a, 2), 4.05 (1H, d, J = 2.8 Hz, H-3a), 4.01 (1H, td, J = 7.9, 5.6 Hz, H-3), 2.79 (1H, dd, J = 16.4, 5.4 Hz, H-4a), 2.50 (1H, dd, J = 16.2, 8.0 Hz, H-4b); ^{13}C NMR (101 MHz, MeOD) δ 159.29, 157.96, 157.71, 155.89, 155.65, 154.88, 154.84, 146.13, 132.14, 131.57, 129.03, 120.02, 116.10, 115.74, 115.20, 101.40, 96.80, 96.12, 82.53, 77.30, 72.59, 68.75, 37.66, 28.51; HR-TOF-ESI-MS m/z 585.1383 $[M + Na]^+$ (calcd for $C_{30}H_{26}O_{11}Na$, 585.1373); The ^{1}H and ^{13}C NMR spectra and mass spectrum are given in the Supporting Data File.

4.5. DPPH and ABTS Assays. For the DPPH assay, stock solutions of the tested compounds were prepared in MeOH with concentrations of 100 μg mL^{-1}. From these stock solutions, dilution series were prepared in microwell plates, obtaining concentration ranges from 252.7 μM to 100.45 nM. This was achieved by transferring 50 μL of the stock solution into the initial well and subsequently diluting it with an equal volume of MeOH. Then, 50 μL of DPPH solution at a concentration of 200 μM were added to each well. After 30 min of incubation, the UV extinctions were measured at 517 nm (free radical DPPH) using a Thermo Scientific microplate reader.

For the ABTS assay, the tested compounds were prepared in MeOH with concentrations of 100 μg mL^{-1}. Then, a dilution series of test compounds ranging from 44.47 μM to 86.86 nM were prepared in MeOH. The $ABTS^{\bullet+}$ solution was generated by mixing potassium persulfate solution (2.5 mM) with ABTS-phosphate-buffered saline (PBS) solution (7.0 mM) in a volume ratio of 1:1, followed by incubation in darkness for 12 to 16 h. After that, the $ABTS^{\bullet+}$ solution was diluted with PBS to achieve an absorbance of 0.7 at 734 nm. It was then kept in darkness for 30 min before use. Then, 150 μL of $ABTS^{\bullet+}$ solution and 100 μL of the dilution series of test compounds were mixed and incubated in the dark for 30 min. After 30 min of incubation, the UV extinctions were measured at 734 nm by a Thermo Scientific microplate reader. The EC_{50} values were calculated using the online tool from www.ic50.tk. The potent antioxidant ascorbic acid (100 μg mL^{-1} in MeOH) was used for comparison in both assays.

4.6. DCFH-DA Assay. Subconfluent SW480 colon carcinoma cells were trypsinized for 5 min in a humidified incubator at 37 °C and under an atmosphere containing 5% CO_2 in air. MEM (Sigma-Aldrich) supplemented with 10%

https://doi.org/10.1021/acsomega.4c03865
ACS Omega 2024, 9, 33888−33899

heat-inactivated FCS (fetal calf serum; BioWest), 1 mM sodium pyruvate, 4 mM L-glutamine, and 1% v/v nonessential amino acid solution was added to stop trypsinization, and cells were centrifuged for 3 min at 1200 rpm (Thermo Scientific, Megafuge 1.0R). After aspiration of the supernatant, the cell pellet was resuspended in supplemented MEM. Afterward, SW480 cells were seeded in 100 μL aliquots in densities of 2.5 $\times$ 10^4 cells/well in 96-well clear flat-bottom microplates. After incubation for 24 h, cells were washed with 200 μL of Hanks' balanced salt solution (HBSS; Sigma-Aldrich; supplemented with 1% heat-inactivated FCS). Then, cells were incubated with 100 μL/well of 25 μM 2′,7′-dichlorofluorescin diacetate (DCFH-DA; in supplemented HBSS) for 45 min at 37 °C. After washing the cells with 200 μL of supplemented HBSS, serially diluted test compounds in phenol-red-free Opti-MEM (Gibco) supplemented with 1% heat-inactivated FCS were added in 200 μL triplicates, and TBHP (*tert*-butylhydroperoxide) was applied as positive control. Immediately after the addition of test compounds, fluorescence (ex/em = 485/516 nm) was measured every 10 min for a total period of 2 h with a microplate reader (BioTek, Synergy HT). Blank-corrected values were calculated relative to negative controls (treated with drug-free supplemented Opti-MEM) from three independent experiments.

4.7. Cytotoxicity Assay. The cytotoxicity of isolated compounds **2**, **3**, **5**, **6**, and **7** was screened on their cytotoxicity in six human cancer cell lines, colon cancer (HT-29), oral cavity carcinoma (KB), breast cancer (MCF-7), cervical cancer (HeLa), hepatocellular carcinoma (HepG-2), and leukemia (P388) using the MTT assay.[22] Screening was performed at compound concentrations of 100 μg mL^{-1}. In order to find the IC_{50} value, concentrations of isolated compounds were evaluated, ranging between 6.25 and 100 μg mL^{-1}. Initially, the cancer cell lines were plated in 96-well plates for 24 h before treatment with isolated compounds. After 24 h of treatment, 10 μL of MTT solution were added to each well and incubated for another 4 h at 37 °C. After the addition of 10% SDS solution (100 μL) into each well, the OD value was measured at 595 nm by a plate reader. Each reaction was measured in triplicates. The IC_{50} values of compounds **3** and **7** were calculated by GraphPad Prism 5.0.

4.8. Docking Studies. *4.8.1. Receptor and Ligand Preparation.* The crystal structure of glutathione reductase (GR) was obtained from the Protein Data Bank (PDB: ID 2gh5),[26] and then, any missing hydrogens were inserted to finalize the structure. The force field for GR atomistic simulation is AMBER99SB, which is designed to be applicable across a broad range of protein and enzyme structures.[27] The structure of GR was energetically minimized using the steepest descent and subsequently refined through the conjugate gradient method until the root-mean-square (RMS) of the energy gradient reached below 0.05 (kcal/mol/Å). For compound ligands, the compound molecule structures were optimized using the B3LYP hybrid functional and a double-ζ polarized basis set with six d-type Cartesian Gaussian polarization functions (6-31G(d,p)),[28] as provided by the Gaussian 09 software package. The ANTECHAMBER[29] was used to perform compatible AMBER force field parameters for specific modification molecules.

4.8.2. Simulation Details and Analysis. Molecular interactions between GR and compounds were observed through atomistic molecular dynamics (MD) simulations. All MD simulations were carried out using the GROMACS 2020 package.[30] The Berendsen method was employed for pressure and temperature coupling to equilibrate the systems. Subsequently, the Parrinello–Rahman pressure coupling and V-rescale temperature coupling were utilized to establish the system in an NPT ensemble, with a temperature set at 297 K and a pressure constant of 1 atm. Long-range electrostatic interactions were computed using the particle mesh Ewald (PME) method. For bonds involving hydrogen atoms, the LINCS algorithm was applied with a time step of 2 fs. The Lennard–Jones potential was utilized to approximate the van der Waals interaction, and it was considered effective within a range of 1.2 nm.

To observe the binding free energy of the protein with the ligand, molecular mechanics, Poisson–Boltzmann surface area (MM-PBSA)[31] was used to examine the binding free energy of protein–ligand interaction. The binding free energy of the protein with a ligand in a solvent can be evaluated as

$$\Delta G_{\text{binding}} = G_{\text{complex}} - (G_{\text{protein}} + G_{\text{ligand}})$$

where G_{complex} is the total free energy of the protein–ligand complex, and G_{protein} and G_{ligand} are the total free energies of the isolated protein and ligand in a solvent, respectively.[31,32]

The equation remains relevant for diverse biomolecular interactions like protein–protein interactions and protein–DNA complexes, etc. Additionally, the free energy for each individual entity can be expressed as

$$\Delta G_x = \langle G_{\text{MM}} \rangle - TS + \langle G_{\text{solvation}} \rangle$$

where x represents the protein, ligand, or the protein–ligand complex. $\langle G_{\text{MM}} \rangle$ denotes the average molecular mechanics potential energy in a vacuum. TS refers to the entropic contribution to the free energy in a vacuum, where T and S represent the temperature and entropy, respectively. The final term, $\langle G_{\text{solvation}} \rangle$, signifies the free energy of solvation. $\langle G_{\text{MM}} \rangle$ encompasses the energy arising from both bonded and nonbonded interactions, and its calculation is derived from the molecular mechanics (MM) force-field parameters.[33,34]

$$\langle G_{\text{MM}} \rangle = E_{\text{bond}} + E_{\text{nonbond}} = E_{\text{bond}} + (E_{\text{vdW}} + E_{\text{elec}})$$

The term E_{bond} represents bonded interactions, encompassing bond, angle, dihedral, and improper interactions. Nonbonded interactions (E_{nonbond}) comprise both electrostatic (E_{elec}) and van der Waals (E_{vdW}) interactions, which are described using Coulomb and Lennard-Jones (LJ) potential functions, respectively. The solvation-free energy ($G_{\text{solvation}}$) is defined as the sum of the following two terms

$$G_{\text{solvation}} = G_{\text{polar}} + G_{\text{nonpolar}}$$

where G_{polar} and G_{nonpolar} represent the electrostatic and nonelectrostatic components contributing to the solvation-free energy, respectively.[35]

■ ASSOCIATED CONTENT

Supporting Information

The Supporting Information is available free of charge at https://pubs.acs.org/doi/10.1021/acsomega.4c03865.

^{1}H NMR, ^{13}C NMR, COSY, TOCSY, HSQC, HMBC, NOESY, HR-ESI-MS, UV, and FTIR spectrum of compounds **1**, **2**, and **6**, and ^{1}H NMR, ^{13}C NMR, and HR-ESI-MS spectrum of isolated compounds and *in silico* data study (PDF)

https://doi.org/10.1021/acsomega.4c03865
ACS Omega 2024, 9, 33888−33899

AUTHOR INFORMATION

Corresponding Author

Weerasak Songoen − *Central Laboratory and Greenhouse Complex, Research and Academic Service Center, Faculty of Agriculture at Kamphaeng Saen, Kasetsart University, Nakhon Pathom 73140, Thailand;* orcid.org/0000-0002-4517-1677; Email: fagrwss@ku.ac.th

Authors

Dominik Wenisch − *Institute of Inorganic Chemistry, Faculty of Chemistry, University of Vienna, A-1090 Vienna, Austria*

Michael A. Jakupec − *Institute of Inorganic Chemistry, Faculty of Chemistry, University of Vienna, A-1090 Vienna, Austria;* orcid.org/0000-0001-7945-1426

Witthawat Phanchai − *Department of Physics, Faculty of Science, Khon Kaen University, Khon Kaen 40002, Thailand;* orcid.org/0000-0002-1319-0793

Siriphan Sukkhaeng − *Central Laboratory and Greenhouse Complex, Research and Academic Service Center, Faculty of Agriculture at Kamphaeng Saen, Kasetsart University, Nakhon Pathom 73140, Thailand*

Lothar Brecker − *Department of Organic Chemistry, University of Vienna, A-1090 Vienna, Austria*

Johann Schinnerl − *Department of Botany and Biodiversity Research, University of Vienna, A-1030 Vienna, Austria;* orcid.org/0000-0003-4494-8736

Sorachat Tharamak − *Department of Chemistry and Center of Excellence for Innovation in Chemistry, Special Research Unit for Advanced Magnetic Resonance, Faculty of Science, Kasetsart University, Bangkok 10900, Thailand*

Wanchai Pluempanupat − *Department of Chemistry and Center of Excellence for Innovation in Chemistry, Special Research Unit for Advanced Magnetic Resonance, Faculty of Science, Kasetsart University, Bangkok 10900, Thailand*

Complete contact information is available at: https://pubs.acs.org/10.1021/acsomega.4c03865

Author Contributions

W.S., D.W., and Wi.P.: writing original draft. W.S., Wa.P., L.B., and J.S.: conceptualization. W.S., S.S., S.T., D.W., and Wi.P.: validation and investigation. D.W.: formal analysis. W.S., M.A.J., D.W., and Wa.P., L.B. and J.S.: writing—review and editing. W.S.: corresponding author.

Notes

The authors declare no competing financial interest.

ACKNOWLEDGMENTS

This work was supported by the Kasetsart University Research and Development Institute (KURDI), Grant Number YF (KU)31.66; the Central Laboratory and Greenhouse Complex, Research and Academic Service Center, Faculty of Agriculture at Kamphaeng Saen, Kasetsart University, Kamphaeng Saen Campus; the Center of Excellence for Innovation in Chemistry (PERCH−CIC), Ministry of Higher Education, Science, Research and Innovation; and the Department of Chemistry, Faculty of Science, Kasetsart University. The analysis of optical rotation of isolated compounds was kindly supported by the Department of Chemistry, Faculty of Science, Silpakorn University.

REFERENCES

(1) Zerega, N. J. C.; Supardi, M. N. N.; Motley, T. J. Phylogeny and Recircumscription of Artocarpeae (Moraceae) with a Focus on *Artocarpus*. *Syst. Bot.* **2010**, *35*, 766−782.

(2) Aneklaphakij, C.; Bunsupa, S.; Sirichamorn, Y.; Bongcheewin, B.; Satitpatipan, V. Taxonomic Notes on the 'Mahat' (*Artocarpus lacucha* and *A. thailandicus*, Moraceae) Species Complex in Thailand. *Plants* **2020**, *9*, No. 391.

(3) Saowakon, N.; Soonklang, N.; Wanichanon, C.; Sobhon, P. The anthelmintic effects of *Artocarpus lakoocha* stem extract on *Fasciola gigantica*. *Planta Med.* **2019**, *85*, No. 1429.

(4) Jagtap, U. B.; Bapat, V. A. *Artocarpus*: A review of its traditional uses, phytochemistry and pharmacology. *J. Ethnopharmacol.* **2010**, *129*, 142−166.

(5) Boonyaketgoson, S.; Rukachaisirikul, V.; Phongpaichit, S.; Trisuwan, K. Deoxybenzoin and flavan derivatives from the twigs of *Artocarpus lakoocha*. *Phytochem. Lett.* **2019**, *31*, 96−100.

(6) Puntumchai, A.; Kittakoop, P.; Rajviroongit, S.; Vimuttipong, S.; Likhitwitayawuid, K.; Thebtaranonth, Y. Lakoochins A and B, New Antimycobacterial Stilbene Derivatives from *Artocarpus lakoocha*. *J. Nat. Prod.* **2004**, *67*, 485−486.

(7) Sritularak, B.; Tan, K.; Likhitwitayawuid, K.; Lipipun, V. New 2-Arylbenzofurans from the Root Bark of *Artocarpus lakoocha*. *Molecules* **2010**, *15*, 6548−6558.

(8) Sritularak, B.; Tantrakarnsakul, K.; Lipipun, V.; Likhitwitayawuid, K. Flavonoids with Anti-HSV Activity from the Root Bark of *Artocarpus lakoocha*. *Nat. Prod. Commun.* **2013**, *8*, 1079−1080, DOI: 10.1177/1934578X1300800.

(9) Songoen, W.; Phanchai, W.; Brecker, L.; Wenisch, D.; Jakupec, M. A.; Pluempanupat, W.; Schinnerl, J. Highly Aromatic Flavan-3-ol Derivatives from Palaeotropical *Artocarpus lacucha* Buch.-Ham Possess Radical Scavenging and Antiproliferative Properties. *Molecules* **2021**, *26*, No. 1078.

(10) Tengamnuay, P.; Pengrungruangwong, K.; Pheansri, I.; Likhitwitayawuid, K. *Artocarpus lakoocha* heartwood extract as a novel cosmetic ingredient: evaluation of the *in vitro* anti-tyrosinase and *in vivo* skin whitening activities. *Int. J. Cosmet. Sci.* **2006**, *28*, 269−276.

(11) Radapong, S.; Chan, K.; Sarker, S. D.; Ritchie, K. J. Oxyresveratrol Modulates Genes Associated with Apoptosis, Cell Cycle Control and DNA Repair in MCF-7 Cells. *Front. Pharmacol.* **2021**, *12*, No. 694562.

(12) Likhitwitayawuid, K.; Sritularak, B.; Benchanak, K.; Lipipun, V.; Mathew, J.; Schinazi, R. F. Phenolics with antiviral activity from *Millettia erythrocalyx* and *Artocarpus lakoocha*. *Nat. Prod. Res.* **2005**, *19*, 177−182.

(13) Chatsumpun, N.; Chuanasa, T.; Sritularak, B.; Lipipun, V.; Jongbunprasert, V.; Ruchirawat, S.; Ploypradith, P.; Likhitwitayawuid, K. Oxyresveratrol: Structural Modification and Evaluation of Biological Activities. *Molecules* **2016**, *21*, No. 489.

(14) Lanez, E.; Saidi, M.; Lanez, T. Assessment of antioxidant and DPPH free radical scavenging activity of 1,2-dithiole-3-thione derivatives by using cyclic voltammetry, spectroscopic, and molecular docking studies. *J. Sulfur Chem.* **2023**, *44*, 542−558.

(15) Couto, N.; Wood, J.; Barber, J. The role of glutathione reductase and related enzymes on cellular redox homoeostasis network. *Free Radic. Biol. Med.* **2016**, *95*, 27−42.

(16) Sangeet, S.; Khan, A. An *in-silico* approach to identify bioactive phytochemicals from *Houttuynia cordata* Thunb. As potential inhibitors of human glutathione reductase. *J. Biomol. Struct. Dyn.* **2023**, 1−20.

(17) Cai, X.-H.; Bao, M.-F.; Zhang, Y.; Zeng, C.-X.; Liu, Y.-P.; Luo, X.-D. A New Type of Monoterpenoid Indole Alkaloid Precursor from *Alstonia rostrata*. *Org. Lett.* **2011**, *13*, 3568−3571.

(18) Yu, J.; Cao, Y.; Song, H.; Wang, X.; Yao, S. Calculations of optical rotation: Influence of molecular structure. *J. Serb. Chem. Soc.* **2012**, *77*, 887−898.

(19) Hatano, T.; Yoshikado, N.; Taniguchi, S.; Kasajima, N.; Ohashi, F.; Shibata, T.; Yoshida, T. Uncariagambiriine and Gambircatechol:

Novel Constituents of *Uncaria gambir* Leaves. *Heterocycles* **2009**, *77*, 793−800.
(20) Taniguchi, S.; Kuroda, K.; Doi, K.; Tanabe, M.; Shibata, T.; Yoshida, T.; Hatano, T. Revised structures of gambiriins A1, A2, B1, and B2, chalcane-flavan dimers from gambir (*Uncaria gambir* extract). *Chem. Pharm. Bull.* **2007**, *55*, 268−272.
(21) Nonaka, G.; Nishioka, I. Novel Biflavonoids, Chalcan-flavan Dimers from Gambir. *Chem. Pharm. Bull.* **1980**, *28*, 3145−3149.
(22) Peng, Y.; Lou, L. L.; Liu, S. F.; Zhou, L.; Huang, X. X.; Song, S. J. Antioxidant and anti-inflammatory neolignans from the seeds of hawthorn. *Bioorg. Med. Chem. Lett.* **2016**, *26*, 5501−5506.
(23) Wolfe, K. L.; Liu, R. H. Structure−Activity Relationships of Flavonoids in the Cellular Antioxidant Activity Assay. *J. Agri. Food Chem.* **2008**, *56*, 8404−8411.
(24) Platzer, M.; Kiese, S.; Herfellner, T.; Schweiggert-Weisz, U.; Miesbauer, O.; Eisner, P. Common Trends and Differences in Antioxidant Activity Analysis of Phenolic Substances Using Single Electron Transfer Based Assays. *Molecules* **2021**, *26*, No. 1244.
(25) Deponte, M. Glutathione catalysis and the reaction mechanisms of glutathione-dependent enzymes. *Biochim. Biophys. Acta, Gen. Subj.* **2013**, *1830*, 3217−3266.
(26) Yu, S. C.; Kim, I. C.; Ri, K. J.; Ri, J.; Kühn, H. New insight into the role of glutathione reductase in glutathione peroxidase-like activity determination by coupled reductase assay: Molecular Docking Study. *J. Inorg. Biochem.* **2021**, *215*, No. 111276.
(27) Showalter, S. A.; Brüschweiler, R. Validation of Molecular Dynamics Simulations of Biomolecules Using NMR Spin Relaxation as Benchmarks: Application to the AMBER99SB Force Field. *J. Chem. Theory Comput.* **2007**, *3*, 961−975.
(28) Songoen, W.; Brunmair, J.; Traxler, F.; Wieser, V. C.; Phanchai, W.; Pluempanupat, W.; Brecker, L.; Schinnerl, J. Yellow Twig (*Nauclea orientalis*) from Thailand: Strictosamide as the Key Alkaloid of This Plant Species. *Molecules* **2022**, *27*, No. 5176.
(29) Wang, J.; Wang, W.; Kollman, P. A.; Case, D. A. Automatic atom type and bond type perception in molecular mechanical calculations. *J. Mol. Graph Model.* **2006**, *25*, 247−260.
(30) Spinello, A.; Lapenta, F.; De March, M. The avidin-theophylline complex: A structural and computational study. *Proteins* **2023**, *91*, 1437−1443.
(31) Kumari, R.; Kumar, R.; Lynn, A. g_mmpbs—A GROMACS Tool for High-Throughput MM-PBSA Calculations. *J. Chem. Inf. Model.* **2014**, *54*, 1951−1962.
(32) Srinivasan, J.; Cheatham, T. E.; Cieplak, P.; Kollman, P. A.; Case, D. A. Continuum Solvent Studies of the Stability of DNA, RNA, and Phosphoramidate−DNA Helices. *J. Am. Chem. Soc.* **1998**, *120*, 9401−9409.
(33) Gohlke, H.; Kiel, C.; Case, D. A. Insights into Protein−Protein Binding by Binding Free Energy Calculation and Free Energy Decomposition for the Ras−Raf and Ras−RalGDS Complexes. *J. Mol. Biol.* **2003**, *330*, 891−913.
(34) Lindorff-Larsen, K.; Piana, S.; Palmo, K.; Maragakis, P.; Klepeis, J. L.; Dror, R. O.; Shaw, D. E. Improved side-chain torsion potentials for the Amber ff99SB protein force field. *Proteins: Struct., Funct., Bioinf.* **2010**, *78*, 1950−1958.
(35) Still, W. C.; Tempczyk, A.; Hawley, R. C.; Hendrickson, T. Semianalytical treatment of solvation for molecular mechanics and dynamics. *J. Am. Chem. Soc.* **1990**, *112*, 6127−6129.

https://doi.org/10.1021/acsomega.4c03865
ACS Omega 2024, 9, 33888−33899